A ONE-DIMENSIONAL FINITE-ELEMENT BOUNDARY-LAYER MODEL WITH A VERTICAL ADAPTIVE GRID

T. M. DUNBAR, E. HANERT AND R. J. HOGAN

July 1, 2008

Abstract

A one-dimensional atmospheric boundary-layer model is developed using the finite element method and a 1.5 order *e-l* turbulence closure scheme. A vertical adaptive strategy is implemented, based upon an heuristic error estimator that depends upon properties of the layer, such as the stratification. The model is used to simulate a moderately stratified stable boundary layer as described in the GABLS (GEWEX Atmospheric Boundary-Layer Study, GEWEX is the Global Water and Energy Cycle Experiment) first intercomparison project, and then a more complicated diurnal cycle, as used in the GABLS Second Intercomparison Project. In the stable boundary-layer experiment, it is shown that including the adaptive strategy can improve the performance of the model such that the error in the model is significantly less (greater than an order of magnitude with an effective resolution of 8 m) than that of the model without adaptivity. The model's turbulence closure scheme and the adaptivity strategy also successfully simulate the different stability regimes present in the diurnal cycle simulation, and represented all of the expected features.

Keywords: Diurnal cycle, *e-l* Turbulence closure, Finite element method, Stable atmospheric boundary layer, Vertical adaptivity

1 Introduction

Recently, the representation of the boundary layer in large scale atmospheric models has become the subject of increased study by projects such as the GEWEX Atmospheric Boundary-Layer Study (GABLS). GABLS has carried out intercomparisons of the boundary-layer representation within GCMs and research models; a first GABLS experiment looked at the case of a moderately stable nocturnal boundary layer (SBL) (Holtslag, 2005), and now a second GABLS experiment is studying a diurnal cycle simulation based upon data from the CASES-99 boundary-layer study. These intercomparisons have thus far shown that the boundary layer is generally poorly represented within operational and climate models (Cuxart et al., 2005), largely to do with deficiencies in the representation of mixing in the turbulence schemes, but it has also been suggested that more resolution may simply be required in order to achieve satisfactory results (Steeneveld et al., 2006). While advances in processing technology are rapidly increasing the potential for such higher resolution models, other methods are possible, for example the technique of adaptive grid refinement.

The adaptive grid refinement method, or the ability to dynamically change the resolution of a numerical model, is widely used in engineering applications and has also been used extensively in ocean models, e.g. Piggott et al. (2004). As the accuracy of the model is changed locally, optimum use of

processing power can be achieved. Their potential for use in atmospheric models is substantial, given the multi-scale nature of atmospheric processes. Several studies of the use of adaptive techniques in atmospheric modeling have previously been attempted, for example, Dietachmayer and Droegemeier (1992), Jablonowski (2004), and Fiedler and Trapp (1993). These studies have tended to concentrate upon two-dimensional flows of phenomena in the horizontal plane, generally using finite difference or finite volume methods. Several different approaches have been used, from grid-nesting to more complex adaptive refinement techniques (ART) such as the continuous dynamic grid adaption (CDGA) method developed by Dietachmayer and Droegemeier (1992). These techniques are employed in order to improve the accuracy of models as well as their efficiency, although results have been mixed. For example, Dietachmayer and Droegemeier (1992) modelled a rising thermal in three dimensions and found that including CDGA in their model increased not only the accuracy of the model, but also the order of convergence of some parameters. On the other hand, Fiedler (2002) used this method in a single column boundary-layer model to investigate its effects upon entrainment compared to other non-adaptive models. While including adaptivity improved the model's results, it was not by any significant amount, and as using such a method would involve much 'tuning' of the adaptive method to fit the situation, it was felt that this would render it impractical for use in larger scale models. Clearly much work is required for these methods to become viable for wide-scale use in meteorological models.

In this study, a one-dimensional boundary-layer model is developed based on the finite element water column model of Hanert et al. (2006), which was originally developed for investigating adaptivity in the ocean. The model use an heuristic error function in order to dynamically adapt the model's grid, such that it follows structures within the flow of the model. For example, the grid can be adapted in order to provide maximum resolution in regions of high shear or stratification, a common strategy within other adaptive techniques. This ensures that any features in the flow, such as jets or temperature inversions, are represented with the optimum accuracy whilst maintaining a computationally efficient simulation.

The accuracy of the model is initially tested using a simple stably stratified test case based upon the Large Eddy Simulation (LES) study by Kosovic and Curry (2000), the details of which are discussed later. This is the test case used in the first GABLS experiment, and so there is a wealth of modelled data available for comparison purposes in Cuxart et al. (2005) and Beare et al. (2005). The adaptive process is then investigated using this simple case, and its performance is assessed qualitatively using an objective error measure. In order to test further the adaptive capabilities of the model, a more complex diurnal cycle is then investigated, following the second GABLS experiment which in turn is based upon observations gathered during the CASES-99 boundary-layer study. The more complex study provides a more challenging test for the adaptive method.

2 Model Description

2.1 Model Equations

The model simulates the evolution of a one-dimensional, horizontally homogeneous, dry boundary layer. No radiation scheme or surface coupling scheme is considered for the sake of simplicity; the model is forced entirely by the geostrophic wind and a prescribed temperature at the surface and there is no mean vertical wind or horizontal divergence. The model equations are derived from the Reynolds-averaged Navier-Stokes equations by using the hydrostatic assumption and the Boussinesq approximation:

$$\frac{\partial\theta}{\partial t} = \frac{\partial}{\partial z}\left(K_h\frac{\partial\theta}{\partial z}\right), \tag{1}$$

$$\frac{\partial U}{\partial t} = \frac{\partial}{\partial z}\left(K_m\frac{\partial U}{\partial z}\right) + f\left(U - U_g\right), \tag{2}$$

$$\frac{\partial V}{\partial t} = \frac{\partial}{\partial z}\left(K_m\frac{\partial V}{\partial z}\right) - f\left(V - V_g\right), \tag{3}$$

where the prognostic variables are the potential temperature, θ, and the horizontal wind components, U and V. K_h and K_m are the heat and momentum eddy diffusivities respectively, f is the Coriolis factor and U_g and V_g are the components of the geostrophic wind. These equations are solved over the model domain, which runs vertically from $z = 0$ to $z = z_{top}$. Eqs. (1)-(3) have to satisfy the following boundary conditions:

$$\begin{aligned}
\theta\big|_{z=0} &= f_\theta(t), \\
K_h\frac{\partial\theta}{\partial z}\big|_{z=z_{top}} &= 0, \\
(U,V)\big|_{z=0} &= (0,0), \\
K_m\frac{\partial}{\partial z}(U,V)\big|_{z=z_{top}} &= (0,0),
\end{aligned}$$

where f_θ is a prescribed function indicating the rate of cooling or warming at the surface.

The turbulence closure scheme used is a 1.5-order scheme with a diagnostic length-scale equation, commonly known as an *e-l* closure, similar to the scheme developed in Andre et al. (1978). In this type of scheme, turbulent fluxes are related to vertical gradients in the flow via eddy diffusivities, which are calculated using the turbulent kinetic energy. An extra prognostic equation is therefore introduced in order to calculate the turbulent kinetic energy e, using the square of the turbulent velocity scale $q^2 = 2e$:

$$\frac{\partial q^2}{\partial t} = 2K_u M^2 - 2K_h N^2 - \frac{2q^3}{16.6l} + \frac{\partial}{\partial z}\left(K_e\frac{\partial q^2}{\partial z}\right), \tag{4}$$

where $K_e = 0.2lq$ is the eddy diffusivity of the turbulent energy and l is the turbulent mixing length scale. This is calculated using a diagnostic equation based on that of Blackadar (1962):

$$\frac{1}{l} = \frac{1}{kz} + \frac{1}{\lambda}, \tag{5}$$

where λ is a limiting mixing length that is generally set to a neutral value, e.g. 40 m. M and N are the Prandtl and Brunt-Väisälä frequencies:

$$\left(M^2, N^2\right) = \left(\left(\frac{\partial U}{\partial z}\right)^2 + \left(\frac{\partial V}{\partial z}\right)^2, \frac{g}{\theta_0}\frac{\partial\theta}{\partial z}\right). \tag{6}$$

The turbulent kinetic energy is then used to parameterise the eddy diffusivities in Eqs. (1)-(3), which can be expressed as:

$$K_m = lqS_m, \tag{7}$$
$$K_h = lqS_h, \tag{8}$$

where S_m and S_h are dimensionless stability functions, which have been parameterised by Galperin et al. (1988) as:

$$S_m = \frac{0.393 - 3.085G_h}{1 - 40.803G_h + 212.469G_h^2}, \tag{9}$$
$$S_h = \frac{0.494}{1 - 34.676G_h}, \tag{10}$$

where G_h is a function of the Brunt-Väisälä frequency:

$$G_h = -\frac{l^2N^2}{q^2}. \tag{11}$$

Constraints are introduced for several of the variables in order to eliminate numerical errors and also to ensure physically satisfying solutions. A minimum value of 1×10^{-5} m^2 s^{-1} is imposed for the momentum, heat and turbulent kinetic energy diffusivities, which corresponds approximately to molecular values of diffusion. A minimum value is also imposed upon the turbulent kinetic energy of 5×10^{-7} m^2 s^{-2}.

2.2 Finite Element Discretisation

Eqs. (1)-(3) are discretized by means of the finite element method (FEM) in a similar fashion to that in Hanert et al. (2006). The derivation of the discrete equations is done in two steps. First of all, the weak formulation of the model's equations is derived. This is achieved by multiplying each equation by some weight function and then integrating by parts over the whole domain. For instance, the weak form of Eq. (1) reads

$$\begin{aligned}\int_0^{z_{top}} \frac{\partial\theta}{\partial t}\hat{\theta}\,\mathrm{d}z &= \int_0^{z_{top}} \frac{\partial}{\partial z}\left(K_h\frac{\partial\theta}{\partial z}\right)\hat{\theta}\,\mathrm{d}z \\ &= -\int_0^{z_{top}} K_h\frac{\partial\theta}{\partial z}\frac{\partial\hat{\theta}}{\partial z}\,\mathrm{d}z + \underbrace{\left(K_h\frac{\partial\theta}{\partial z}\hat{\theta}\right)\Big|_{z=z_{top}}}_{=0} - \left(K_h\frac{\partial\theta}{\partial z}\hat{\theta}\right)\Big|_{z=0},\end{aligned} \tag{12}$$

where $\hat{\theta}$ is a suitable weighting function. It can be seen that the integration by parts of the diffusion term allows us to naturally incorporate the Neumann boundary conditions in the weak formulation.

The second step consists of building a discrete approximation of the exact solution θ. The discrete solution, denoted θ^h, is defined on a partition of the domain into a set of non-overlapping intervals, usually called elements. The partition of the domain into elements is called a grid. The size of these elements can vary in both space and time. The discrete solution is then defined as:

$$\theta^h(z,t) = \sum_{j=1}^{n} \theta_j(t)\phi_j(z), \tag{13}$$

where n denotes the number of velocity degrees of freedom. In this study, the unknown nodal values θ_j are lying on the grid vertices and the corresponding basis functions ϕ_j are piecewise linear polynomials equal to one on node j and zero on all the other nodes (i.e. triangular shaped functions). Higher order basis functions could be used as well but will not be considered here. The nodal values are found by replacing θ by θ^h and $\hat{\theta}$ by ϕ_i for $(1 \leq i \leq n)$ in Eq. (12). The following set of discrete equations is then obtained:

$$\int_0^{z_{top}} \frac{\partial \theta^h}{\partial t}\phi_i \, \mathrm{d}z = -\int_0^{z_{top}} K_h \frac{\partial \theta^h}{\partial z}\frac{\partial \phi_i}{\partial z} \, \mathrm{d}z - (K_h \frac{\partial \theta^h}{\partial z}\phi_i)\Big|_{z=0}. \tag{14}$$

Finally, by using (13), one may rewrite Eq. (14) in matrix form:

$$\mathsf{M}_{ij}\frac{\mathrm{d}\theta_j}{\mathrm{d}t} = \mathsf{D}_{ij}\theta_j, \tag{15}$$

where $\mathsf{M}_{ij} = \int_0^{z_{top}} \phi_i\phi_j \, \mathrm{d}z$ is the mass matrix and:

$$\mathsf{D}_{ij} = -\int_0^{z_{top}} K_h \frac{\partial \phi_i}{\partial z}\frac{\partial \phi_j}{\partial z} \, \mathrm{d}z + (K_h\phi_i \frac{\partial \phi_j}{\partial z})\Big|_{z=0}, \tag{16}$$

is the stiffness matrix. These integrals are easily computed as they only involve products of low order polynomials or products of their derivatives. The last step consists of discretizing Eq. (15) in time by using a standard finite difference time stepping scheme. The discretization of Eqs. (2)-(3) is similar.

2.3 Grid Adaptation

The use of the finite element method makes the inclusion of an adaptive scheme easy to implement, as it allows the use of non-uniform grids that are permitted to adapt in space and time. The basic idea behind the adaptive method is to compute an error estimation for a given discrete solution, and then modify the grid in order to evenly distribute the error over the model's domain. In other words, resolution is increased where the error estimator is large and is decreased where the error is small. Rather than review all the theory on which adaptive methods stand, we refer the reader to the paper by Piggott et al. (2004) and the references therein for more information.

In this work, we present a simple example of adaptivity based on an heuristic error measure; it will depend upon the stratification and the second derivative of the potential temperature in the boundary layer. Following Burchard and Beckers (2004), the non-dimensional error on the numerical solution may be defined as:

$$\begin{aligned} \varepsilon^h = \quad & c_1 \quad \frac{\theta^h}{\max(\theta^h)} + c_2 \frac{\| \underline{u^h, v^h} \|}{\max(\| \underline{u^h, v^h} \|)} + c_3 \frac{| \frac{\partial \theta^h}{\partial z} | - \theta_z^*}{\max(| \frac{\partial \theta^h}{\partial z} | - \theta_z^*)} + \cdots \\ & c_4 \quad \frac{\| \frac{\partial \underline{u^h, v^h}}{\partial z} \|}{\max(\| \frac{\partial \underline{u^h, v^h}}{\partial z} \|)} + c_5 \frac{| \frac{\partial^2 \theta^h}{\partial z^2} |}{\max(| \frac{\partial^2 \theta^h}{\partial z^2} |)} + \cdots \end{aligned} \tag{17}$$

The error estimator is constructed from separate terms, each relating to different properties of the boundary layer. In Eq. (17), the terms on the right hand side respectively represent the potential temperature, wind speed, temperature stratification and the wind shear. It is, of course, possible to define the error estimation to depend upon other properties of the layer, such as the second derivative of the velocity component. These can be simply implemented by adding extra terms to Eq. (17), although these are not considered in this paper. Constant values can be added to improve the estimator, for example, the value (θ_z^*) represents the potential temperature lapse rate above the boundary layer. For this model, this is a constant value and so to help prevent unwanted movement of the grid in this area, it was found useful to subtract this value from the error. Each term is also normalised by its maximum value in the layer. The terms are then weighted using the c_x values, such that their relative effects upon the adaptivity can be altered.

As an example, an error estimator could be defined which would increase the resolution of the grid in regions of high stratification, such as the inversion at the top of the layer, or near the surface where a stable or unstable layer may be forming. This would involve setting c_1, c_2, c_4 and c_5 to zero, so that the only remaining term is that related to the stratification, $\mid \partial\theta/\partial z \mid$. Again, we stress that this error estimator is very heuristic, and is only based upon our knowledge of the physical phenomena within the boundary layer.

In order to achieve the largest possible advantage from using the adaptive procedure it was found useful to include smoothing techniques to prevent oscillations in the grid due to rapid changes in the grid's structure. When computing the new positions of the nodes within the grid, a relaxation term was added to take into account the previous position of the node, while a Laplacian smoothing technique was used for the error estimator. These smoothing methods do not incur any significant computational cost to the model.

Once an error measure has been derived, the nodes may be redistributed accordingly. As the accuracy of the finite element method can depend both on the order of the basis functions and the grid resolution, several strategies exist to uniformly distribute the interpolation error. One procedure, p-adaptivity, locally increases or decreases the degree of the finite element approximation. It is also possible to modify the accuracy of the numerical scheme by changing the grid resolution. This might be achieved by either moving the nodes location or by locally changing the grid and its connectivity. The former method, refered to as r-adaptivity, does not change the topology and keeps the number of elements constant while the latter, refered to as h-adaptivity, adds and removes elements from the grid. When the number of elements remains the same, the movement of the grid may be taken into account by adding an advection term in the equations. The goal of this term is to counterbalance the movement of the grid nodes and the advection velocity is simply the opposite of the grid velocity. When the number of elements changes, grid-to-grid interpolation is required.

In this work, we consider only the r-adaptive methods. As mentioned previously, it requires the introduction of a transport term in the discrete equations to compensate for the motion of the grid. If the grid nodes are at positions $z_i(t)$ for $(1 \leq i \leq n)$, the vertical velocity at which a grid node moves is: $w_i(t) = dz_i/dt$. A continuous grid velocity field w^h may then be built by linearly interpolating between grid velocity nodal values. For instance, the modified temperature equation reads:

$$\int_0^{z_{top}} \frac{\partial \theta^h}{\partial t}\phi_i \, \mathrm{d}z - \int_0^{z_{top}} w^h \frac{\partial \theta^h}{\partial z}\phi_i \, \mathrm{d}z \quad = \quad - \int_0^{z_{top}} K_h \frac{\partial \theta^h}{\partial z}\frac{\partial \phi_i}{\partial z} \, \mathrm{d}z - (K_h \frac{\partial \theta^h}{\partial z}\phi_i)\Big|_{z=0}. \tag{18}$$

In matrix form, this yields:

$$\mathsf{M}_{ij}\frac{d\theta_j}{dt} - \mathsf{A}_{ij}\theta_j = \mathsf{D}_{ij}\theta_j, \tag{19}$$

where $\mathsf{A}_{ij} = \int_0^{z_{top}} w^h \phi_i \frac{\partial \phi_j}{\partial z} \, \mathrm{d}z$ is the additional advection matrix.

An example of r-adaptation is shown in Fig. 1. We start with a grid $\{z_i,\ 1 \leq i \leq n\}$ and a piecewise constant error field $\varepsilon(z)$. We compute the error integral on each element: $E_i = \int_{z_i}^{z_{i+1}} \varepsilon(z) \, \mathrm{d}z$ and on the whole domain: $E_{tot} = \sum_{i=1}^{n-1} E_i$. The new grid $\{z_i^*,\ 1 \leq i \leq n\}$ is then built by imposing the following constraints:

$$E_i^* = \int_{z_i^*}^{z_{i+1}^*} \varepsilon(z) \, \mathrm{d}z = \frac{E_{tot}}{n-1}, \tag{20}$$

$$z_0^* = z_0, \tag{21}$$

$$z_n^* = z_n. \tag{22}$$

This is achieved by successively moving the inner nodes of the initial grid.

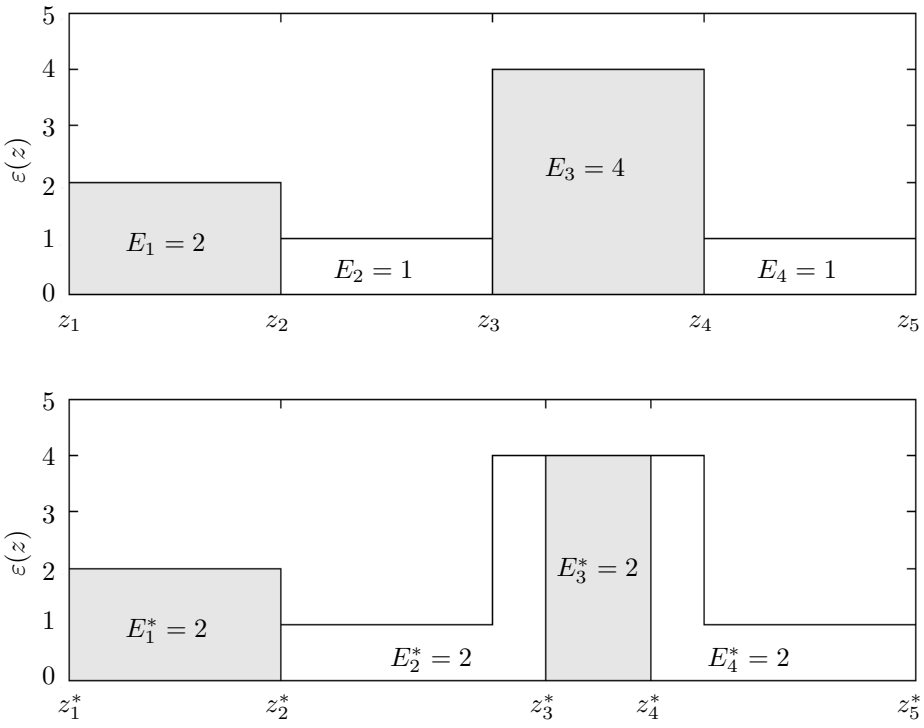

Figure 1: Example of grid adaptation. The initial grid $\{z_i,\ 1 \leq i \leq 5\}$ is composed of 4 elements of unit length (top). By using an r-adaptive procedure, a new grid $\{z_i^*,\ 1 \leq i \leq 5\}$ is obtained where the error ($e(z)$) is evenly distributed (bottom).

3 Results and Discussion

3.1 Stable Boundary Layer Experiment

As a verification experiment the model was run using the specifications for the first GABLS experiment, which is based upon the Kosovic and Curry (2000) stable nocturnal boundary-layer simulations. In this case the boundary layer is moderately stratified, and the initial state and forcings are based upon observations from the BASE study in 1994. As mentioned previously, the simulation is driven by an imposed barotropic geostrophic wind, with a specified surface cooling rate. In this particular case, the layer reaches a quasi-steady state after a few hours of simulation (i.e. the potential temperature profile is changing at a constant rate while all other mean flow properties have reached a steady, unchanging state). Although the conditions are based upon a field study from the Arctic regions, this type of layer is not uncommmon in the atmosphere; it is similar to a classic nocturnal boundary layer. The strong geostrophic wind forcing in this scenario allows radiative forcing to be safely ignored.

The initial temperature profile consists of an adiabatic layer with potential temperature 265 K from the surface up to 100 m, above which the air is stable with a constant lapse rate of 0.01 K m^{-1}. A prescribed cooling rate of 0.25 K hr^{-1} is enforced at the surface while at the upper boundary the temperature is fixed at 268 K, the temperature of the free atmosphere above. Wind profiles are initially set equal to the geostrophic wind value (8 m s^{-1} in the x-direction) throughout the layer, at the surface no-slip conditions are applied and at the top of the layer the wind is forced to its geostrophic value. A typical turbulent kinetic energy profile is initialised as decreasing linearly from 0.4 m^2 s^{-2} to zero from the surface up to a height of 250 m; above this it is equal to an imposed minimum value. A Dirichlet boundary condition is used at the surface, where the turbulent kinetic energy is forced to $q_0^2 = B_1^{2/3} u_*^2$ (Mellor and Yamada (1974)), and at the upper boundary is set to its minimum value. The surface friction velocity is defined as:

$$u_* = -\left[\left(\overline{u'w'}\right)_0^2 + \left(\overline{v'w'}\right)_0^2\right]^{\frac{1}{4}} = -\sqrt{K_u \left|\frac{\partial U}{\partial z}\right|} \tag{23}$$

The model domain is 400 m deep and the simulation is run over a period of 9 hours with the timestep set to 20 seconds.

The simulation is performed at 73^{o}N, corresponding to a Coriolis parameter of $f = 1.39 \times 10^{-4}$ s^{-1}, and the surface has a roughness length $z_0 = 0.1$ m. As recommended by Beare et al. (2005) and Cuxart et al. (2005), the limiting value of the turbulent mixing length λ is set to 10 m. This is consistent with mixing lengths estimated from observations of stable layers, and serves to reduce the over-mixing that causes some models to under-represent details of the layer such as the nocturnal jet or upper-level inversion.

The adaptive scheme implemented for testing in this scenario used r-adaptivity, with the error estimator depending only upon the gradient and second derivative of the potential temperature within the layer as in Eq. 17 (i.e. the weighting values used were: $c_1 = 0, c_2 = 0, c_3 = 1, c_4 = 0, c_5 = 1$). This was felt to be the most useful criterion for this experiment, as it ensures that the accuracy of the model is enhanced at the upper-level inversion and near the surface. θ_z^* was set to 0.01 K m^{-1} to account for the constant lapse rate above the inversion, and prevent the adaptivity from moving the grid into this region.

Potential temperature and wind profiles after eight hours of of the simulation are shown in Fig. 2. These are compared to a high resolution, three-dimensional Large Eddy Simulation from Beare et al. (2005), which has been shown to be in good agreement with observed values. The finite element model was run twice, with and without the adaptive procedure implemented. In order to prevent large jumps

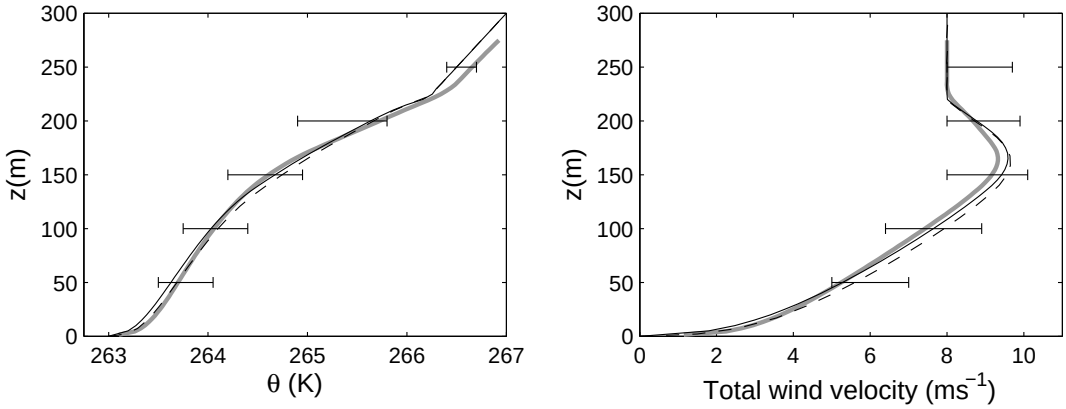

Figure 2: Potential temperature and total wind velocity profiles of the SBL experiment after eight hours of integration. The finite-element model was run with and without the adaptive procedure operating, as represented by the solid and dashed lines respectively; the non-adaptive run had 80 elements in the model, the adaptive run had 40. The thick grey line represents results from an LES model as described in Beare et al. (2005). The error bars represent the maximum spread of other operational and research-based one-dimensional model results taken from the first GABLS experiment as described by Cuxart et al. (2005).

in the model resolution at the start of the adaptive simulation, the grid was generated with more of the elements clustered around the initial position of the temperature inversion, at 100 m.

The model results are close to those obtained by the LES models, and are well within the range of the other one-dimensional models tested by Cuxart et al. (2005). The temperature profile at lower levels and through the mixed layer is very similar to the profile of the LES results, whilst the upper level inversion at the boundary layer top is well defined. The nocturnal jet is of comparable strength to that of the LES results, and occurs at a nearly identical level. Of particular note is that the model captures these features, which many other 1-D models, even those with similar closure schemes, fail to simulate (Cuxart et al. (2005)).

In order to quantify the effect that the adaptive process is having on the simulation, the L_2 error is calculated with respect to a high resolution reference solution. This is similar to the root-mean-squared fractional error; it gives a measurement of the difference between the model results and a very high resolution model. The high resolution reference case was run with the adaptive process switched off, a resolution of 1 m (corresponding to 400 elements over the domain) and a timestep of 5 seconds in order to minimise numerical errors. The relative 'L_2 error' on θ^h is defined as follows:

$$L_2(\theta^h) \quad = \quad \sqrt{\frac{\int_0^{z_{top}} (\theta^r - \theta^h)^2 \, \mathrm{d}z}{\int_0^{z_{top}} (\theta^r)^2 \, \mathrm{d}z}}, \tag{24}$$

where the superscript r denotes the high resolution model run, and h the model run under investigation. Other variables can be investigated simply by substituting for θ.

The model was then run again with and without the adaptive procedure, for a range of numbers of elements. Figure 3 shows the L_2 error for the different model runs, calculated for the potential temperature and the total wind velocity. Lines 1 and 2 in the plots show the slope representing a quadratic convergence of the error. It can be seen that for the non-adaptive model runs, an increase in the number of elements in the grid shows a convergence towards the reference solution (a decrease in

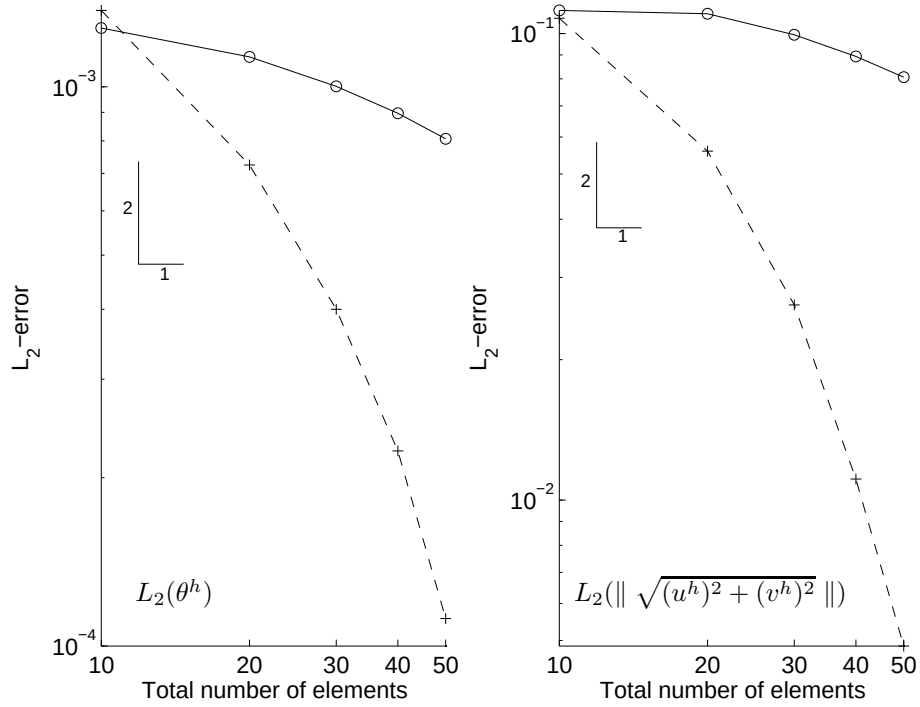

Figure 3: L_2 error plots showing the errors associated with the potential temperature (left) and total wind velocity profiles (right) after 9 hours of simulation of a stable boundary layer, for the finite element model run with (+) and without (∘) the adaptive procedure implemented when compared to a reference solution with a resolution of 1 m, which corresponds to a grid with 400 elements. With the adaptive procedure implemented in the model, the rate of convergence of the error is quadratic, whereas without the adaptive procedure the error convergence is less than linear.

the error), although this convergence is much less than linear. By including the adaptive procedure, the model converges much more quickly, at nearly quadratic rates, and also has a much smaller error.

Although not shown in Fig. 3, it has been seen previously that if more elements are included in the grid, then the convergence of the error for the adaptive model runs begins to decrease. This is due to an inherent error incurred by the movement of the grid as it adapts, which increases with the number of elements. Eventually, this error will outweigh the benefits of including the adaptive grid, and so adaptivity would be of more use in coarser grids, such as those used in NWP models, where even in leading models there are often less than 50 levels for the whole atmosphere. We would normally expect quadratic convergence in the error, however certain flaws in the representation of the boundary layer prevent this. For example, in order to accurately simulate the logarithmic profiles in the surface layer, we would require a resolution of the same order as the roughness length, which is equal to 0.1 m. Our model resolutions ranging from 40 m − 5 m are not sufficient to capture this. Possible solutions to this problem could be to include a free-slip boundary condition at the surface, or utilising logarithmic shape functions in the bottom element rather than linear ones, as suggested by Hanert et al. (2007).

3.2 Diurnal Cycle Experiment

As a further test scenario for the adaptive procedure, the diurnal cycle from the GABLS Second Intercomparison project was used. This is based on observations between 23 and 25 of October 1999 from the

CASES99 field study in Kansas, USA, which were taken during a period with clear skies and when there was minimal change in the synoptic situation. The diurnal temperature cycle that was used to force the model at the surface can be found at: `http://people.su.se/~gsven/gabls/`. This case was previously studied by Poulos et al. (2002) and has been successfully modelled by Steeneveld et al. (2006) using a very high resolution one-dimensional model which also included radiation and surface feedback processes. Again, the situation is simplified for this model in order to concentrate upon the effect of adaptivity, and so the model is forced by the surface temperature only.

Time-height contour plots of the prognostic variables in the model are shown in Figure 4, along with a plot of the changing heights of the nodes in the model with the adaptive scheme implemented. Several features of the boundary layer development are worth mentioning. The evolution of the temperature profile shows the slow growth of the nocturnal layer, and then the rapid growth of the convective daytime layer through this, with entrainment occurring at the top of the boundary layer. The wind profile reveals the growth of the nocturnal jet and the reduction of the wind speed during the day due to turbulence increasing friction throughout the layer. The turbulent kinetic energy is clearly seen to peak during the day when convection is at its most vigorous, and extends through the boundary layer, whilst it is subdued during the night. Enhanced turbulent kinetic energy can be seen at the top of the boundary layer where entrainment is occurring, and also in early morning when the convective layer is growing through the night-time mixed layer. These plots are similar in appearance to those in comparable modelling studies, such as Mellor and Yamada (1974), and Liu and Leung (1998). Figure 4 (d) shows how the adaptive process has adjusted the grid; resolution has been enhanced at the top of the boundary layer and near the surface, and is higher within the nocturnal and convective layers than the free atmosphere. However, the adaptive strategy used does not work so well during the day/night transition, and the ensuing rapid changes in temperature gradient cause oscillation in the grid which are transmitted above the boundary layer. This emphasises the need to choose the error estimator carefully; in this experiment the estimator is based upon a priori knowledge of the dynamics of the system being studied. The estimator could be made more general and versatile by using a method which does require prior knowledge of the system.

4 Conclusions

A one-dimensional finite element boundary layer model has been presented using a 1.5-order e-l turbulence closure scheme. The performance of the model in simulating a stable boundary layer has been investigated by comparison with a LES and several other 1-D turbulence closure models. The model results were found to be in good agreement with the LES model results, and were well within the bounds of other turbulence closure schemes.

An adaptive grid refinement scheme was introduced into the model. This was designed in order to change the resolution of the model according to features in the potential temperature profile in order to increase the resolution of the model in regions of higher stratification, such as the inversion at the boundary layer top. The impact of this scheme upon the model was tested by simulating the test case from the first GABLS intercomparison (Cuxart et al. (2005)). The adaptive procedure was shown to reduce the error in the model substantially for coarse grids, and also increased the convergence rate of the error. The model was also used to simulate the diurnal cycle from the second GABLS intercomparison experiment. Although the turbulence closure scheme used was not configured for us in convective situations, the model performed well and simulated all the expected features of the flow. The adaptive procedure showed that it is potentially suitable for use in diurnal simulations, and while this particular adaptive approach needs further work if it is to be used to improve the accuracy of the model, this improvement is certainly achieveable.

This type of procedure could be very useful within research models for which computing power is at a premium. For example, it could provide a computationally cheap improvement to models when

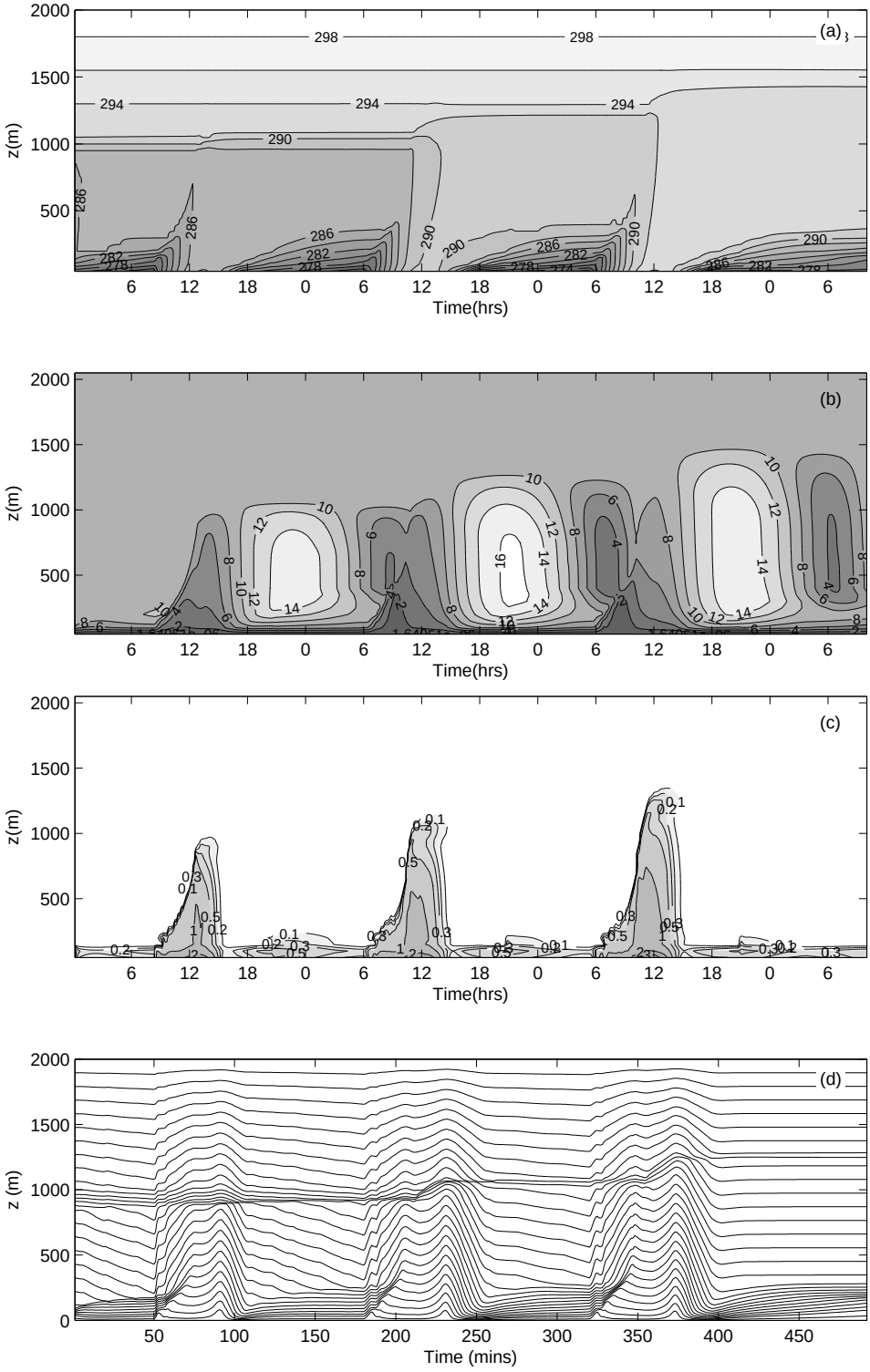

Figure 4: Time-height contour plots of the prognostic variables and the node height positions over 82 hours of integration of the second GABLS experiment diurnal case. (a) Potential temperature (K), (b) total wind velocity (ms^{-1}, (c) turbulent kinetic energy ($\mathrm{m}^2\mathrm{s}^{-2}$) and (d) node height positions. For (a), (b) and (c) the model was run at a resolution of 50m (40 elements) without adaptivity, while the node height positions plot (d) is from a model run with 30 elements using r-adaptivity depending upon the gradient of potential temperature. This number of elements was chosen to provide a clearer image of the moving grid nodes.

studying boundary layer processes, which could then yield simpler or more accurate parameterisations for use within full weather and climate models. Further study is however required to investigate the benefits in efficiency that this approach can bring, which have not been discussed in this paper. For example, at what point does the increased computing power required to include the adaptive procedure outweigh the increase in accuracy of the solution? For larger scale models, such as those used in weather forecasting, adaptive procedures could potentially bring a similar benefit. however, significant work would be required in order to implement such procedures, and this must be weighed against the benefits.

5 Acknowledgements

We would like to thank the Department of Meteorology at the University of Reading for providing the funding which ensured that this work could be done.

References

Andre, J. C., G. De Moor, G. Therry, and R. Du Vachat: 1978, 'Modelling the 24-Hour Evolution of the Mean and Turbulent Structures of the Planetary Boundary Layer'. *J Atmos Sci* **35**, 1861–1883.

Beare, R. J., M. MacVean, A. Holtslag, I. E. Cuxart, J., J.-C. Golaz, M. Jimenez, M. Khairoutdinov, B. Kosovic, D. Lewellen, T. Lund, J. Lundquist, A. McCabe, A. Moene, Y. Noh, S. Raasch, and P. Sullivan: 2005, 'An Intercomparison Of Large-Eddy Simulations Of The Stable Boundary Layer'. *Boundary-Layer Meteorol* **118**(2), 247–272.

Blackadar, A. K.: 1962, 'The Vertical Distribution of Wind and Turbulent Exchange in a Neutral Atmosphere'. *J Geophys Res* **67**, 3095–3102.

Burchard, H. and J.-M. Beckers: 2004, 'Non-Uniform Adaptive Vertical Grids In One-Dimensional Numerical Ocean Models'. *Ocean Modelling* **6**, 51–81.

Cuxart, J., A. Holtslag, R. Beare, E. Bazile, A. Beljaars, A. Cheng, L. Conangla, M. Ek, F. Freedman, R. Hamdi, H. Kerstein, A.; Kitagawa, G. Lenderink, D. Lewellen, J. Mailhot, T. Mauritsen, V. Perov, G. Schayes, G.-J. Steeneveld, G. Svensson, P. Taylor, W. Weng, S. Wunsch, and K.-M. Xu: 2005, 'Single-Column Model intercomparison For A Stably Stratified Atmospheric Boundary Layer'. *Boundary-Layer Meteorol* **118**(2), 273–303.

Dietachmayer, G. and K. K. Droegemeier: 1992, 'Application of Continuous Dynamic Grid Adaption Techniques to Meteorological Modelling: Part I: Basic formulation and accuracy'. *Mon Wea Rev* **120**, 1675–1706.

Fiedler, B. H.: 2002, 'Grid Adaption And Its Effect On Entrainment in an *E-l* Model of the Atmospheric Boundary Layer'. *Mon Wea Rev* **130**, 733–740.

Fiedler, B. H. and R. J. Trapp: 1993, 'A Fast Dynamic Grid Adaption Scheme for Meteorological Flows'. *Mon Wea Rev* **121**, 2879–2888.

Galperin, B., L. H. Kantha, S. Hassid, and S. Rosati: 1988, 'A Quasi-Equilibrium Turbulent Energy Model For Geophysical Flows'. *J Atmos Sci* **45**, 55–62.

Hanert, E., E. Deleersnijder, S. Blaise, and J.-F. Remacle: 2007, 'Capturing the Bottom Boundary Layer in Finite Element Ocean Models'. *Ocean Modelling* **17**, 153–162.

Hanert, E., E. Deleersnijder, and V. Legat: 2006, 'An Adaptive Finite Element Water Column Model Using The Mellor-Yamada Level 2.5 Turbulence Closure Scheme'. *Ocean Modelling* **12**, 205–223.

Holtslag, B.: 2005, 'Preface: GEWEX Atmospheric Boundary Layer Study (GABLS) on Stable Boundary Layers'. *Boundary-Layer Meteorol* **118**(2), 243–246.

Jablonowski, C.: 2004, 'Adaptive Grids In Weather And Climate Modelling'. Ph.D. thesis, The University Of Michigan.

Kosovic, B. and J. A. Curry: 2000, 'A Large Eddy Simulation Of A Quasi-Steady, Stably-Stratified Atmospheric Boundary Layer'. *Journal Of The Atmospheric Sciences* **57**, 1052–1068.

Liu, C. H. and D. Y. C. Leung: 1998, 'Evaluation of an Atmospheric Boundary Layer Model Used for Air Pollution Studies'. *Journal Of Applied Meteorology* **37**, 1561–1576.

Mellor, G. L. and T. Yamada: 1974, 'A Heirarchy Of Turbulence Closure Models For Planetary Boundary Layers'. *J Atmos Sci* **31**, 1791–1806.

Piggott, M. D., C. C. Pain, G. J. Gorman, P. W. Power, and A. J. H. Goddard: 2004, '*h, r* and *hr* adaptivity with applications in numerical ocean modelling'. *Ocean Modelling* **10**, 95–113.

Poulos, S. G., W. Blumen, D. C. Fritts, J. K. Lundquist, J. Sun, S. P. Burns, C. Nappo, R. Banta, R. Newsom, J. Cuxart, E. Terradellas, B. Balsley, and M. Jensen: 2002, 'CASES-99: A Comprehensive Investigation of the Stable Nocturnal Boundary Layer'. *Bull Amer Meteorol Soc* **83**, 555–581.

Steeneveld, G. J., B. J. H. van de Wiel, and A. A. M. Holtslag: 2006, 'Modelling The Evolution of the Atmospheric Boundary Coupled to the Land Surface for Three Contrasting Nights in CASES99'. *J Atmos Sci* **63**, 920–935.